European Radiology
https://doi.org/10.1007/s00330-018-5381-7

HEAD AND NECK

# MR-based radiomics signature in differentiating ocular adnexal lymphoma from idiopathic orbital inflammation

Jian Guo[1] · Zhenyu Liu[2] · Chen Shen[3] · Zheng Li[1] · Fei Yan[1] · Jie Tian[2,4] · Junfang Xian[1]

Received: 4 September 2017 / Revised: 6 February 2018 / Accepted: 8 February 2018


## Abstract

**Objectives** To assess the value of the MR-based radiomics signature in differentiating ocular adnexal lymphoma (OAL) and idiopathic orbital inflammation (IOI).

**Methods** One hundred fifty-seven patients with pathology-proven OAL (84 patients) and IOI (73 patients) were divided into primary and validation cohorts. Eight hundred six radiomics features were extracted from morphological MR images. The least absolute shrinkage and selection operator (LASSO) procedure and linear combination were used to select features and build radiomics signature for discriminating OAL from IOI. Discriminating performance was assessed by the area under the receiver-operating characteristic curve (AUC). The predictive results were compared with the assessment of radiologists by chi-square test.

**Results** Five radiomics features were included in the radiomics signature, which differentiated OAL from IOI with an AUC of 0.74 and 0.73 in the primary and validation cohorts respectively. There was a significant difference between the classification results of the radiomics signature and those of a radiology resident ($p < 0.05$), although there was no significant difference between the results of the radiomics signature and those of a more experienced radiologist ($p > 0.05$).

**Conclusions** Radiomics features have the potential to differentiate OAL from IOI.

**Key Points**

- *Clinical and imaging findings of OAL and IOI often overlap, which makes diagnosis difficult.*
- *Radiomics features can potentially differentiate OAL from IOI non invasively.*
- *The radiomics signature discriminates OAL from IOI at the same level as an experienced radiologist.*

**Keywords** Radiomics · Inflammation · Lymphoma · Orbital neoplasms · Magnetic resonance imaging (MRI)

**Abbreviations**

| | |
|---|---|
| ADC | Apparent diffusion coefficient |
| AUC | Area under the ROC curve |
| DCE | Dynamic contrast enhanced |
| DWI | Diffusion-weighted imaging |
| ETL | Echo train length |
| FS | Fat saturation |
| FSE | Fast spin echo |
| GLCM | Grey level co-occurrence matrix |
| GLRLM | Grey level run length matrix |
| ICC | Intraclass correlation coefficient |
| IOI | Idiopathic orbital inflammation |
| LASSO | Least absolute shrinkage and selection operators procedure |
| MRI | Magnetic resonance imaging |
| NEX | Number of excitations |
| OAL | Ocular adnexal lymphoma |
| ROC | Receiver-operating characteristic |
| SRHGE | Short-run high-grey emphasis |
| T1WI | T1-weighted images |

Jian Guo and Zhenyu Liu contributed equally to this work.

✉ Jie Tian
jie.tian@ia.ac.cn

✉ Junfang Xian
cjr.xianjunfang@vip.163.com

[1] Department of Radiology, Beijing Tongren Hospital, Capital Medical University, No. 1 of Dongjiaominxiang, Dongcheng District, Beijing 100730, China

[2] CAS Key Laboratory of Molecular Imaging, Institute of Automation, Beijing 100190, China

[3] School of Life Science and Technology, Xidian University, Xi'an, Shanxi 710126, China

[4] University of Chinese Academy of Sciences, Beijing 100049, China

Published online: 09 April 2018

| | |
|---|---|
| T2WI | T2-weighted image |
| TE | Echo time |
| TR | Repetition time |

## Introduction

Ocular adnexal lymphoma (OAL) is the most common orbital malignant neoplasm in adults [1–4] and local radiotherapy is the first-line treatment [5, 6]. Idiopathic orbital inflammation (IOI) remains the third most common orbital disease, following after thyroid-associated orbitopathy and lymphoproliferative disease [7], and oral corticosteroids are the mainstay of treatment [8, 9]. The clinical and imaging findings of these entities often overlap, and a biopsy may be needed to provide tissue diagnosis [10, 11]. As biopsy is an invasive process with known risks and the biopsy tract may remain afterwards, this method is also discommodious for lesions of the orbital apex and those around the optic nerve [5, 12, 13]. It is desirable to seek alternative noninvasive diagnostic confirmation to guide appropriate treatment.

MRI is the preferred modality for evaluating orbital masses [14]. Some reported MRI findings (such as the tumour location, signal intensity on T2-weighted imaging (T2WI), moulding sign and contrast enhancement characteristics) are useful in separating OAL from IOI [15–17]. There are, however, other studies reporting the limitations of these diagnostic characteristics [12, 18]. Diffusion-weighted imaging (DWI) and dynamic contrast-enhanced (DCE) MRI were also used to characterise orbital masses and to distinguish OAL from IOI, albeit with a partial overlap [19–24]. Most of these studies showed obvious semi-quantitative differences between lesions based on a relatively limited of number of cases [21, 22]. Hence, the conclusions were not always consistent. For example, Sun et al. reported a specificity of 100% for the differentiation of OAL from IOI using ADC [24], while Xu [25] reported specificity of 61.1%. Furthermore, Kapur et al. reported no significant difference in the ADC ratio between OAL and IOI [21]. It can therefore be seen that the literature to date provides limited help in discriminating OAL and IOI. Therefore, the imaging-based differential diagnosis of OAL and IOI still presents substantial room for improvement.

In recent years, the development of machine learning and pattern classification resulted in the growing importance of radiomics [26, 27]. Radiomics refers to the extraction and analysis of large amounts of advanced quantitative imaging features obtained with high throughput from medical images. These quantitative features, which may not be perceptible to human vision, can potentially provide valuable diagnostic, prognostic or predictive information in oncology [28–33]. Recent studies have shown promising results for imaging-extracted textural features in the differential diagnosis of malignant and benign tumours. Most of these reports involve breasts, soft tissue, lymph nodes and head and neck [34–38].

A review of the literature to date shows no reports on the predictive imaging features of orbital masses using radiomics. The aim of this study is to investigate the utility of extracted radiomics features that may help to characterise or discriminate OAL from IOI.

## MATERIALS AND METHODS

### Patients

This retrospective study was approved by our institutional review board and the requirement for informed consent was waived. All patient data and personal information were anonymised prior to analysis.

The study population consisted of 157 (84 OALs and 73 IOIs) patients enrolled consecutively between March 2010 and July 2016. The inclusion criteria were: (1) histopathologically confirmed cases of primary OAL or IOI; (2) patients with orbital MRI (including pre- and post-contrast studies) less than 14 days before biopsy or surgery; (3) patients with no history of surgery or treatment in the affected orbits. The exclusion criteria were as follows: (1) poor image quality such as significant motion or susceptibility artefacts; (2) orbital lesions less than 0.5 cm in short diameter; (3) OAL secondary to systemic lymphoma; (4) patients with IOI or OAL.

The consecutive study population was divided into two groups according to the time points. The first group (recruited from March 2010 to September 2014) consisted of 94 patients (47 OALs and 47 IOIs). They formed the primary cohort of 46 males and 48 females (mean age, 50.55 ± 14.03 years; age range, 5–85 years). The second group (recruited from October 2014 to July 2016) consisted of 63 consecutive patients (37 OALs and 26 IOIs). They constituted the independent validation cohort of 39 males and 24 females (mean age, 55.37 ± 13.36 years; age range, 25–80 years).

### Image data acquisition

All imaging was performed on a 3.0-T Signa HDxt scanner (GE Healthcare) with an eight-channel high-resolution head coil. Pre-contrast axial fast spin-echo (FSE) T1-weighted images (T1WI), T2-weighted images (T2WI) and post-contrast T1WI in the axial and coronal planes were acquired in all cases. The imaging parameters are shown in Table 1. Post-contrast T1WI were obtained after an intravenous bolus injection of 0.1 ml/kg gadopentetate dimeglumine. Chemical shift

**Table 1** MR scanning parameters on the 3.0-T scanner

| Sequence | TR (ms) | TE (ms) | Field of view (mm) | Number of slices | Slice thickness (mm) | Slice gap (mm) | NEX | Acquisition time (min) | Bandwidth (HZ/px) | Matrix | ETL |
|---|---|---|---|---|---|---|---|---|---|---|---|
| T1WI FSE | 400 | 10 | 18*18 | 16 | 3 | 0.3 | 2 | 2'12 | 41.67 | 384*256 | 4 |
| T2WI FSE | 2880 | 120 | 18*18 | 16 | 3 | 0.3 | 2 | 1'32 | 41.67 | 384*256 | 18 |
| Post-contrast $T_1$WI | 400 | 10 | 18*18 | 16 | 3 | 0.3 | 2 | 2'12 | 41.67 | 384*256 | 4 |

*TR* repetition time; *TE* echo time; *NEX* number of excitations; *ETL* echo train length

selective fat saturation (FS) was used in the post-enhancement axial T1WI.

## Image segmentation and feature extraction

Image segmentation was done separately on axial T2WI and post-enhanced T1WI sequences using the open-source ITK-SNAP software (http://www.itksnap.org). Manual free hand delineation of a region of interest (ROI) was performed on a selected slice containing the largest lesion area. Two radiologists (without prior knowledge of the histopathological diagnosis) independently performed segmentation. Radiologist 1 was board certified with 16 years of head and neck imaging experience, while radiologist 2 was a resident with 4 years of head and neck imaging experience.

The ROI outlines were read and processed using a feature quantisation programme developed in house by our institution. Processing was carried out using MATLAB 2014b (MathWorks, USA). Two-dimensional features in the calculation included first-order grey-level statistics (grey-level histograms) and grey-level texture features with and without wavelet filtering. Grey-level texture features included the grey-level run-length matrix (GLRLM) and the grey-level co-occurrence matrix (GLCM) features. Eight hundred six features in total were known to be effective [29].

## Features selection, radiomics signature building and validation

A feature selection method based on the least absolute shrinkage and selection operator (LASSO) was employed to reduce the dimensionality of extracted features. LASSO is a regression analysis method that performs both variable selection and regularisation of high-dimensional data. We adopted the "glmnet" package in R software to fulfil feature selection in the primary cohort. Linear combination of the selected features was used to construct the radiomics signature. The predictive performance of the signature was assessed in the primary cohort and validated in the validation cohort. The area under the receiver-operating characteristic (ROC) curve (AUC) was used to evaluate the predictive performance of the signature in differentiating OAL from IOI. Figure 1 shows the framework for the radiomics workflow.

## Imaging analysis by the radiologists

To compare the diagnostic performance of the radiomics signature with visual assessment, MRIs (pre-contrast T1WI, T2WI and post-contrast T1WI) of all 157 cases were independently reviewed by the same two radiologists that completed image segmentation.

All personal information was de-identified prior to analysis and both radiologists had no prior knowledge of the histopathological results. In addition, they had no access to other functional sequences (including DWI and DCE). Diagnosis was based on image analysis according to their respective clinical experience. The locations of the OAL and IOI were categorised into four groups: intraconal, extraconal, preseptal and multi-compartmental lesions. Diagnostic sensitivity, specificity and accuracy were calculated and compared with the histopathological results.

## Statistical Analysis

Statistical analyses were carried out in R 3.3.0 (R Development Core Team, 2016). The two-sided statistically significant level was set to 0.05. The differences in age and gender distribution between the primary and validation cohorts were compared by means of independent samples t-test and chi-square test respectively (two-tailed, $p < 0.05$). The intraclass correlation coefficients (ICCs) were used to assess agreement of extracted features by two radiologists. Kappa test analyses were performed to determine the inter-observer agreement. The "Glmnet" package was used in feature selection and radiomics signature development. ROC curves were drawn using the "pROC" package. The "Hmisc" and "rms" packages were used in the validation process. All the above-mentioned software packages are subject to the open source GPL v2 license (GNU general public license version 2). The chi-square test was used for the

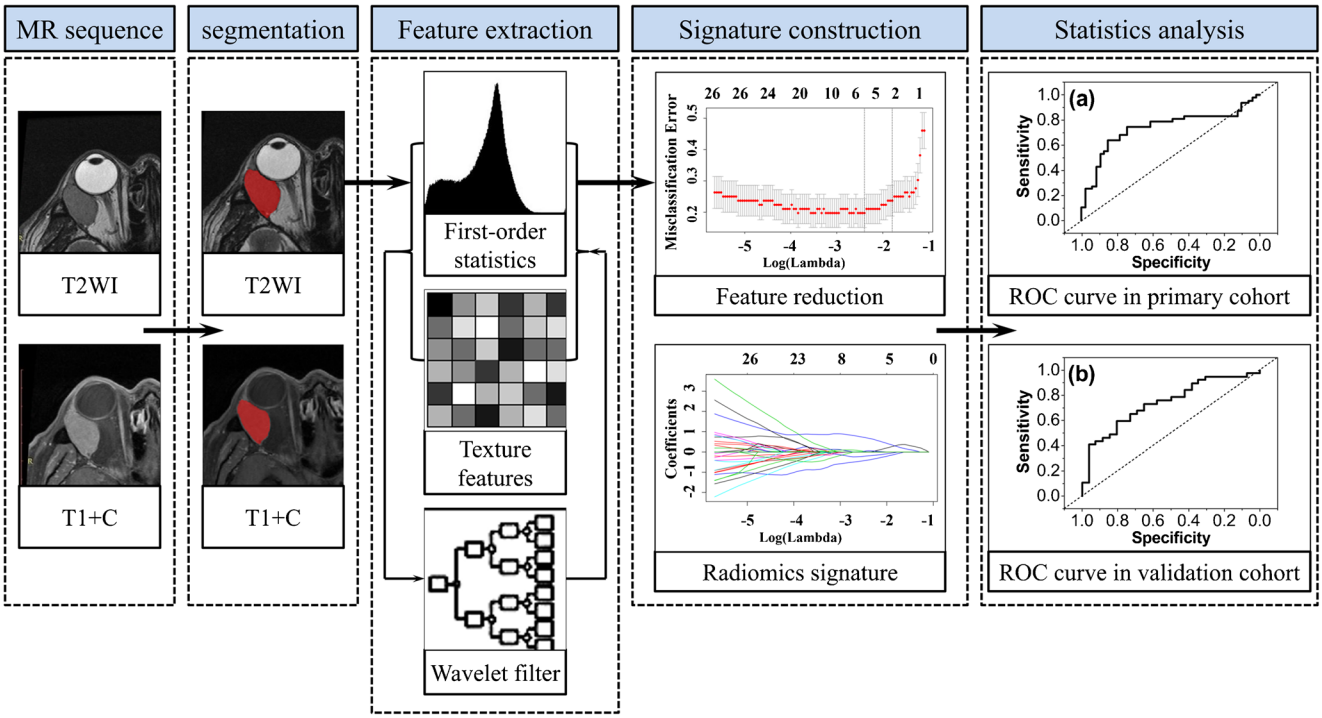


**Fig. 1** The radiomics workflow. Segmentation is performed on MR images to define the tumour region. From this region, the radiomics features are extracted, including grey-level first-order statistics and texture analysis with and without wavelet filtering. Using the least absolute shrinkage and selection operator (LASSO) method, several features were selected to build the radiomics signature. Finally, the classification ability of the radiomics signature was evaluated by the receiver-operating characteristics (ROC) curves obtained in both the training and validation cohorts

statistical analysis of the classified data of the two radiologists and radiomics signatures.

## Results

### Clinical characteristics of the patients

There were significant differences in age and gender distribution between the two diseases ($p < 0.05$) (Table 2). Compared with IOI, OAL has a predilection for older male patients. No significant differences in the clinical characteristics between the two cohorts of OAL and IOI (respectively $p$ = 0.138-0.613) were demonstrated.

### Feature selection, radiomics signature development and diagnostic validation

The ICCs calculated for agreement of features extracted by the two radiologists ranged from 0.763 to 0.895, reflecting good agreement. (The segmentation results of the radiologist with more working experience were used for further analysis). To identify the relevant predictors, all explanatory features extracted from the primary cohort were included in the LASSO logistic regression procedure. Features with

**Table 2** Age and gender distribution of OAL and IOI

| | Primary cohort (94) | | | Validation cohort (63) | | |
|---|---|---|---|---|---|---|
| | OAL | IOI | $p$ | OAL | IOI | $p$ |
| Gender, no. | 47 | 47 | | 37 | 26 | |
| Male | 31 | 15 | 0.002* | 29 | 10 | 0.002* |
| Female | 16 | 32 | | 8 | 16 | |
| Age (mean ± SD, years) | 54.83 ± 12.28 | 46.28 ± 14.49 | 0.003* | 59 ± 13.13 | 50.19 ± 12.13 | 0.009* |

*$p < 0.05$

regression coefficients of zero or close to zero were eliminated. Finally, 5 features (1 grey-level first-order statistical feature, 2 texture features and 2 texture features with wavelet filtering) out of 806 radiomics features were selected to build the predictive model. Among them, four features were based on post-contrast T1WI with fat saturation and one on T2WI. There were significant differences ($p < 0.05$) in feature values of grey-level median, GLCM entropy and GLRLM SRHGE (short-run high-grey emphasis) after wavelet filtering between OAL and IOI in both the primary and validation cohorts (Table 3).

The radiomics signature was constructed (with the five above-mentioned features) by means of linear combination according to their coefficients. The diagnostic performance of the radiomics signature was evaluated using the ROC curve of the primary and validation cohort (Fig. 2). The patient-based diagnostic accuracy of the radiomics signature for the binary classification of OAL or IOI revealed an AUC of 0.74 (95% CI, 0.65 to 0.88) in the primary cohort. The diagnostic validation was done in the independent cohort with an AUC of 0.73 (95% CI, 0.67 to 0.85) (Table 4). Forty-one cases were wrongly classified according to the radiomics signature (Table 5).

## Imaging analysis by the radiologists

Both OAL and IOI can involve one or more orbital compartments. For OAL, disease location was found as follows: intra-conal (8/84, 9.5%); extra-conal (17/84, 20.2%); preseptal compartment (6/84, 7.1%); multi-compartments (53/84, 63.1%). As for IOI, the following was found: intra-conal (4/73, 5.5%); extra-conal (33/73, 45.2%); preseptal compartment (2/73, 2.7%); multi-compartments (34/73, 46.6%).

The diagnostic performance of the MRI visual assessment was evaluated. Sensitivity, specificity and accuracy of the more experienced radiologist, not surprisingly, were higher than those of the radiology resident (Table 4). The accuracies of MRI assessments were 72.61% (experienced radiologist) and 62.42% (radiology resident). Inter-observer agreement showed a kappa value of 0.61 (95% CI 0.553–0.781).

## Comparisons of visual assessment and radiomics signature results

The chi-square test showed a significant difference between the discriminating results of the radiomics signature and those of the radiology resident ($p = 0.039 < 0.05$). There was however no significant difference between the discriminating results of the radiomics signature and those of the experienced radiologist ($p = 0.899 > 0.05$). These findings indicate the radiomics signature has a higher level of performance compared with a resident but achieves a level equivalent to that

**Table 3** Five selected features and feature value analysis in OAL and IOI

| No. | Feature name | Feature type | MR sequence | Feature value in primary cohort | | Feature value in validation cohort | | | |
|---|---|---|---|---|---|---|---|---|---|
| | | | | OAL | IOI | $p$ ($t$ test) | OAL | IOI | $p$ ($t$ test) |
| 1 | Grey-level median | Grey level first-order statistics | Post-contrast T1WI FS | 0.91 ± 0.92 | 0.17 ± 1.05 | 0.007* | 0.96 ± 2.52 | 0.09 ± 2.79 | 0.010* |
| 2 | Sum average GLCM 135° | Texture | Post-contrast T1WI FS | 0.31 ± 0.93 | 0.21 ± 1.06 | 0.267 | 0.48 ± 0.85 | 0.68 ± 0.81 | 0.246 |
| 3 | GLRLM SRHGE after wavelet filter | Wavelet filter | Post-contrast T1WI FS | 0.36 ± 0.51 | 0.36 ± 1.22 | 0.0004* | 0.21 ± 0.64 | 0.19 ± 0.56 | 0.005* |
| 4 | GLCM entropy after wavelet filter | Wavelet filter | Post-contrast T1WI FS | -0.07 ± 0.89 | 0.37 ± 1.06 | 0.0002* | -0.03 ± 0.07 | 0.32 ± 0.57 | 0.003* |
| 5 | Energy GLCM 90° | Texture | T2WI | 2.04 ± 6.21*10-3 | 4.11 ± 5.33*10-3 | 0.891 | 2.81 ± 9.11*10-3 | 3.80 ± 7.12*10-3 | 0.279 |

GLCM grey-level co-occurrence matrix; GLRLM grey-level run-length matrix; SRHGE short-run high-grey emphasis; FS fat saturation; *$p < 0.05$

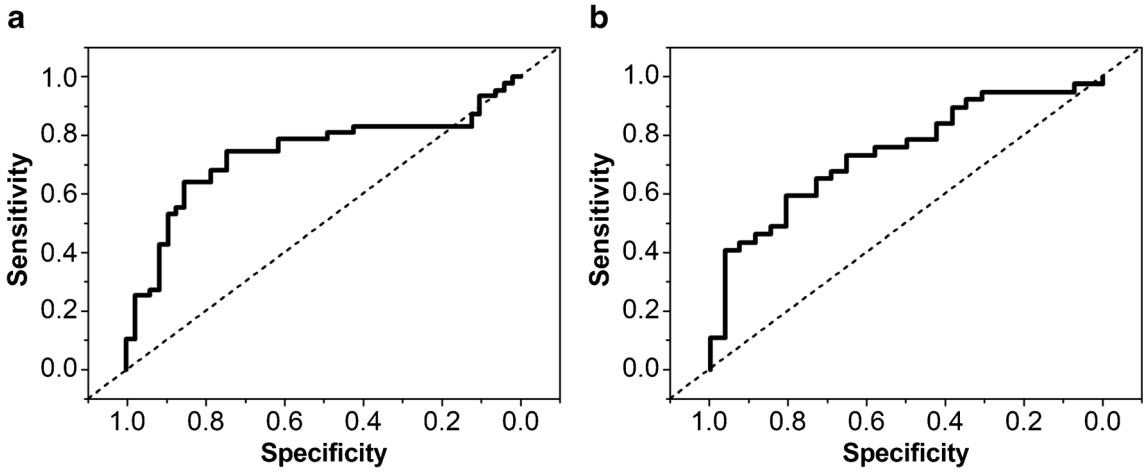


**Fig. 2** Receiver-operating characteristic (ROC) curves for differentiation of OAL and IOI using the radiomics signature in the primary (a) and validation cohorts (b). The areas under ROC curve (AUC) are 0.74 (a) and 0.73 (b) respectively

of an experienced radiologist. Similar results were obtained in both the primary and validation cohorts.

The misjudgement ratio (ratio of the misclassification number and total number of cases for both OAL and IOI) of the radiomics signature was also similar to that of the experienced radiologist but superior to that of the resident in both study cohorts. Table 5 shows the wrongly classified cases by radiomics signature and radiologists (as well as the location of the lesions). It shows that only 15 (34.88%) and 18 (30.51%) cases misclassified respectively by radiologist 1 and radiologist 2 were also misclassified by the radiomics signature.

## Discussion

Distinguishing OAL from IOI based on MRI morphology is challenging (especially in hyper-cellular lesions) [39]. There are often no significant differences in the tumour laterality, shape, location or signal intensity between the benign (mainly IOI cases) and malignant (OAL) orbital lymphoproliferative disorders groups [25]. In the current study, we employed T2WI and post-contrast T1WI to investigate the diagnostic performance of radiomics features in discriminating OAL from IOI. We found that the MR-based radiomics signature was effective in distinguishing OAL from IOI, reaching the level of an experienced radiologist.

The present study shows quantitative image features such as texture analysis can be extracted from T2WI and post-contrast T1WI. This is consistent with findings of other investigators [32, 40, 41]. In our study, image segmentation was done on a single slice showing the largest tumour cross-sectional area. Previous texture analysis studies performed on the largest cross-sectional tumour area have also shown promising results in biological correlates [29, 42, 43] and

**Table 4** Diagnostic performance of the radiomics signature and visual assessment individually for detection of OAL from IOI

| | Radiomics signature | | | | Visual assessment | |
|---|---|---|---|---|---|---|
| | Primary cohort | | Validation cohort | | Radiologist 1 | Radiologist 2 |
| | % (*n*) | 95% CI | % (*n*) | 95% CI | | |
| Sensitivity (%) (*n*) | 72.34% (34/47) | 64.82%, 81.66% | 72.97% (27/37) | 64.90%, 79.22% | 72.62% (61/84) | 60.71% (51/84) |
| Specificity (%) (*n*) | 76.60% (36/47) | 68.11%, 82.23% | 73.08% (19/26) | 65.38%, 85.15% | 72.60% (53/73) | 64.38% (47/73) |
| False positive Rate (%) (*n*) | 23.40% (11/47) | 18.55%, 30.70% | 26.92% (7/26) | 20.45%, 33.40% | 27.40% (20/73) | 35.62% (26/73) |
| False negative Rate (%) (*n*) | 27.66% (13/47) | 20.09%, 36.42% | 27.03% (10/37) | 21.22%, 35.88% | 27.38% (23/84) | 39.29% (33/84) |
| PPV (%) (*n*) | 75.56% (34/45) | 66.36%, 82.55% | 79.41% (27/34) | 71.85%, 87.00% | 75.31% (61/81) | 66.23% (51/77) |
| NPV (%) (*n*) | 73.47% (36/49) | 61.30%, 80.45% | 65.52% (19/29) | 58.06%, 72.30% | 69.74% (53/76) | 58.75% (47/80) |
| Accuracy (%) (*n*) | 74.47% (70/94) | 65.50%, 81.43% | 73.02% (46/63) | 62.70%, 83.52% | 72.61% (114/157) | 62.42% (98/157) |
| AUC | 0.74 | 0.65, 0.88 | 0.73 | 0.67, 0.85 | --- | --- |

CI = confidence interval; PPV = positive predictive value; NPV = negative predictive value; AUC = area under receiver-operating characteristic curve

**Table 5** Location of wrongly classified cases by the radiomics signature and two radiologists

| Wrongly classified cases | Radiomics signature | Radiologist 1 (16 years of experiences) | Radiologist 2 (4 years of experiences) |
|---|---|---|---|
| Intra-conal compartment (%) | 2 (4.88%) | 3 (6.98%) | 5 (8.47%) |
| Extra-conal compartment (%) | 9 (21.95%) | 11 (25.58%) | 15 (25.42%) |
| Preseptal compartment (%) | 2 (4.88%) | 4 (9.30%) | 3 (5.08%) |
| Multi-compartments (%) | 28 (68.29%) | 25 (58.14%) | 36 (61.02%) |
| Total | 41 | 43 | 59 |
| Primary cohort | 24 (25.53%) | 27 (28.72%) | 37 (39.36%) |
| Validation cohort | 17 (26.98%) | 16 (25.40) | 22 (34.92%) |

Misclassified cases mainly involved multi-compartments or the extra-conal compartment by both the radiomics signature and radiologists. However, more than half of cases wrongly classified by the radiomics signature were different from those wrongly classified by the radiologists.

prognostic [44, 45] and predictive [46] potential, thereby demonstrating that these features appear to give a good representation of tumours for certain tasks. Eight hundred six image features (including grey-level first-order statistics and texture features with and without a wavelet filter) were used in our study. Many reports have already shown grey-level histograms and texture features of different imaging modalities were useful in separating benign from malignant masses [34, 35, 38, 47–50]. This study utilised the least absolute shrinkage and selection operators (LASSO) for the reduction of dimensionality. This shrinkage method within linear regression models allows for automatic feature selection and produces sparser solutions [51]. Five descriptive radiomics features were extracted (from MR images of OAL and IOI) to define our model to assess their classification performance and robustness. These features were also found to be useful in head and neck lesions reported by other authors [38, 50].

It is interesting to note that most reports on GLCM entropy after the wavelet filter (one of the selected features in our study) showed higher values in malignant tumours than in benign lesions [35, 38, 52]. However, our study showed the opposite. In information theory, entropy is used to measure the uncertainty or randomness of a random variable [53]. Hence, homogenously enhancing lesions on post-contrast T1WI have lower grey-level entropy compared with heterogeneously enhanced abnormalities. As we know, the histopathology of OAL shows the proliferation of many monoclonal lymphocytes, which on MRI exhibits mild to moderate homogeneous enhancement. On the other hand, IOI displays a more complex variable combination of polymorphous infiltrations composed of mature lymphocytes, plasma cells, eosinophils or macrophages together with reactive fibrosis [39]. It can therefore be seen that the entropy values may provide further information on histopathology, which may be potentially useful in differentiating these two entities.

The predictive performance based on machine learning is also compared with radiologist assessment for the first time. The diagnostic performance of the radiomics signature was better than that of the radiology resident. The accuracy of the radiomics signature (in the primary and validation cohorts) was similar to that of an experienced radiologist. The machine learning classifier can make it to the level of an experienced radiologist in the head and neck. Our radiomics signature appeared stable as almost the same AUC value was obtained in the primary and independent validation cohorts. In a word, the

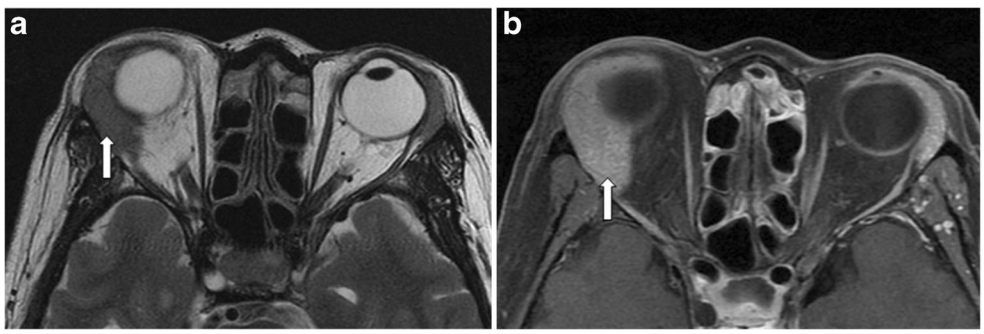


**Fig. 3** A 58-year-old female with IOI in the right lacrimal gland confirmed histologically. Axial T2-weighted image (a) and axial T1-weighted post-contrast fat suppression image (b) show a well-defined enlarged right lacrimal gland (white arrow) with moulding around the eyeball. The lesion is slightly more hyper-intense relative to muscle on T2WI and shows moderate homogenous enhancement. The case was initially misdiagnosed as OAL by visual assessment and the correct diagnosis was predicted by radiomics signature

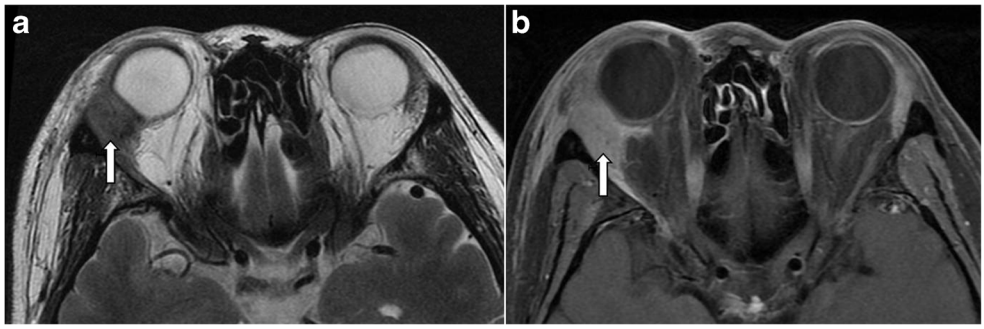


**Fig. 4** A 41-year-old female with IOI in the right lacrimal gland confirmed histologically. Axial T2-weighted image (a) and axial T1-weighted post-contrast fat suppression image (b) show an ill-defined enlarged right lacrimal gland (white arrow) with moulding around the eyeball. The lesion appeared mildly hypo-intense relative to muscle on T2WI and shows moderate homogeneous enhancement. The case was correctly diagnosed as IOI by visual assessment while wrongly classified as OAL by the radiomics signature

results showed that radiomics features derived from medical images were useful in discriminating malignant OAL from benign IOI. The above results are in agreement with other studies [35, 38, 53, 54].

Curiously, both radiomics and radiologists have more difficulties in establishing the correct classification in cases involving multi-compartments or lesions located in the extraconal compartment. However, more than half of cases wrongly classified by the radiomics signature were different from those by radiologists (Figs. 3 and 4). The reasons behind these observations are not immediately clear. The literature shows the ADC value to be of value in discriminating OAL from IOI [20, 22, 25]. According to Sepahdari [55], there were significant differences between the ADC values of orbital lymphoma and inflammatory disease without overlap. Xu on the other hand reported ADCs with a sensitivity of 91% and specificity of 61% [25]. In comparison, our radiomics signature showed lower sensitivity but higher specificity. Although our radiomics signature has a lower sensitivity than the ADC, the higher specificity gives a higher level of confidence in making the correct distinction.

Although our results showed the potential usefulness of the radiomics signature in differentiating OAL from IOI, there are limitations. First, the study was retrospective in nature and did not cover multi-modality medical images. As described above, the inclusion of the ADC value may further improve the utility of the radiomics signature in separating OAL from IOI [20, 22, 25]. Furthermore, we only used the predictive performance of the first- and several second-order grey-level features. Other data and shape features could be included to improve the effectiveness. Second, our results may not be generalisable even though we validated the diagnostic performance of our proposed model in this study. Fruehwald-Pallamar et al. [38, 50] have shown texture-based analysis to be useful in the discrimination of benign and malignant tumours when performed on one scanner with the same protocol, while multicentre studies were not recommended. Thus, the result of present study should be confirmed in other data resources to make the model more credible for generalisation.

In conclusion, our results demonstrate the potential use of radiomics features in differentiating OAL from IOI. The proposed objective model is not expected to replace tissue diagnosis, but may provide an additional tool for improving diagnostic accuracy in the day-to-day work of a radiologist. It may be especially useful for less experienced radiologists or general radiologists with no special training in head and neck imaging.

**Acknowledgements** The authors would like to express their sincere appreciation to all reviewers for their kind comments.

This work was presented in part at the 2017 International Society of Magnetic Resonance Imaging in Medicine Annual Meeting.

**Funding** This study has received funding from the High Level Health Technical Personnel of Bureau of Health in Beijing under grant no. 2014-2-005; Beijing Municipal Administration of Hospitals Clinical Medicine Development of Special Funding Support under grant no. ZYLX201704; Key Talent Project of Beijing under Grant no. 2014001; The Priming Scientific Research Foundation for the Senior Researcher in Beijing Tongren Hospital, Capital Medical University, under grant no. 2016-YJJ-GGL-011.

## Compliance with ethical standards

**Guarantor** The scientific guarantor of this publication is Junfang Xian.

**Conflict of interest** The authors of this manuscript declare no relationships with any companies, whose products or services may be related to the subject matter of the article.

**Statistics and biometry** One of the authors has significant statistical expertise.

**Informed consent** Written informed consent was obtained from all subjects (patients) in this study.

**Ethical approval** Institutional Review Board approval was obtained.

**Methodology**
- retrospective
- diagnostic study
- performed at one institution

## References


1. Rosado MF, Byrne GE, Ding F et al (2006) Ocular adnexal lymphoma: a clinicopathologic study of a large cohort of patients with no evidence for an association with Chlamydia psittaci. Blood 107: 467–472
2. Sjö LD (2009) Ophthalmic lymphoma: epidemiology and pathogenesis. Acta Ophthalmologica 87:1–20
3. Shields JA, Shields CL, Scartozzi R (2004) Survey of 1264 patients with orbital tumors and simulating lesions: The 2002 Montgomery Lecture, part 1. Ophthalmology 111:997–1008
4. Ferreri AJ, Dolcetti R, Du MQ et al (2008) Ocular adnexal MALT lymphoma: an intriguing model for antigen-driven lymphomagenesis and microbial-targeted therapy. Ann Oncol 19:835–846
5. Woolf DK, Ahmed M, Plowman PN (2012) Primary lymphoma of the ocular adnexa (orbital lymphoma) and primary intraocular lymphoma. Clin Oncol (R Coll Radiol) 24:339–344
6. Kharod SM, Herman MP, Morris CG, Lightsey J, Mendenhall WM, Mendenhall NP (2018) Radiotherapy in the management of orbital lymphoma: a single institution's experience over 4 decades. Am J Clin Oncol 41:100–106
7. Shikishima K, Kawai K, Kitahara K (2006) Pathological evaluation of orbital tumours in Japan: analysis of a large case series and 1379 cases reported in the Japanese literature. Clin Exp Ophthalmol 34: 239–244
8. Rubin PA, Foster CS (2004) Etiology and management of idiopathic orbital inflammation. Am J Ophthalmol 138:1041–1043
9. Swamy BN, McCluskey P, Nemet A et al (2007) Idiopathic orbital inflammatory syndrome: clinical features and treatment outcomes. Br J Ophthalmol 91:1667–1670
10. Dagi Glass LR, Freitag SK (2016) Orbital inflammation: Corticosteroids first. Survey of Ophthalmology 61:670–673
11. Mombaerts I, Rose GE, Garrity JA (2016) Orbital Inflammation: Biopsy first. Survey of Ophthalmology 61:664-669
12. Cytryn AS, Putterman AM, Schneck GL, Beckman E, Valvassori GE (1997) Predictability of magnetic resonance imaging in differentiation of orbital lymphoma from orbital inflammatory syndrome. Ophthal Plast Reconstr Surg 13:129–134
13. Haradome K, Haradome H, Usui Y et al (2014) Orbital lymphoproliferative disorders (OLPDs): value of MR imaging for differentiating orbital lymphoma from benign OPLDs. AJNR Am J Neuroradiol 35:1976–1982
14. Xian J, Zhang Z, Wang Z et al (2010) Value of MR imaging in the differentiation of benign and malignant orbital tumors in adults. Eur Radiol 20:1692–1702
15. Warner MA, Weber AL, Jakobiec FA (1996) Benign and malignant tumors of the orbital cavity including the lacrimal gland. Neuroimaging Clin N Am 6:123–142
16. Roshdy N, Shahin M, Kishk H et al (2010) MRI in diagnosis of orbital masses. Curr Eye Res 35:986–991
17. Sullivan TJ, Valenzuela AA (2006) Imaging features of ocular adnexal lymphoproliferative disease. Eye 20:1189–1195
18. Uehara F, Ohba N (2002) Diagnostic imaging in patients with orbital cellulitis and inflammatory pseudotumor. Int Ophthalmol Clin 42:133–142
19. Politi LS, Forghani R, Godi C et al (2010) Ocular adnexal lymphoma: diffusion-weighted MR imaging for differential diagnosis and therapeutic monitoring. Radiology 256:565–574
20. Fatima Z, Ichikawa T, Ishigame K et al (2014) Orbital masses: the usefulness of diffusion-weighted imaging in lesion categorization. Clin Neuroradiol 24:129–134
21. Kapur R, Sepahdari AR, Mafee MF et al (2009) MR imaging of orbital inflammatory syndrome, orbital cellulitis, and orbital lymphoid lesions: the role of diffusion-weighted imaging. AJNR Am J Neuroradiol 30:64–70
22. Sepahdari AR, Aakalu VK, Setabutr P, Shiehmorteza M, Naheedy JH, Mafee MF (2010) Indeterminate orbital masses: restricted diffusion at MR imaging with echo-planar diffusion-weighted imaging predicts malignancy. Radiology 256:554–564
23. Purohit BS, Vargas MI, Ailianou A et al (2016) Orbital tumours and tumour-like lesions: exploring the armamentarium of multiparametric imaging. Insights Imaging 7:43–68
24. Sun B, Song L, Wang X et al (2017) Lymphoma and inflammation in the orbit: Diagnostic performance with diffusion-weighted imaging and dynamic contrast-enhanced MRI. J Magn Reson Imaging 45:1438–1445
25. Xu XQ, Hu H, Liu H et al (2017) Benign and malignant orbital lymphoproliferative disorders: differentiating using multiparametric MRI at 3.0T. J Magn Reson Imaging 45:167–176
26. Lambin P, Riosvelazquez E, Leijenaar RTH et al (2012) Radiomics: Extracting more information from medical images using advanced feature analysis. Eur J Cancer 48:441–446
27. Kumar V, Gu Y, Basu S et al (2012) Radiomics: the process and the challenges. Magn Reson Imaging 30:1234–1248
28. Huang Y, Liu Z, He L et al (2016) Radiomics signature: a potential biomarker for the prediction of disease-free survival in early-stage (I or II) non-small cell lung cancer. Radiology 281:947–957
29. Huang YQ, Liang CH, He L et al (2016) Development and validation of a radiomics nomogram for preoperative prediction of lymph node metastasis in colorectal cancer. J Clin Oncol 34:2157–2164
30. Parmar C, Leijenaar RT, Grossmann P et al (2015) Radiomic feature clusters and prognostic signatures specific for lung and head & neck cancer. Sci Rep 5:11044
31. Wang J, Kato F, Oyama-Manabe N et al (2015) Identifying triple-negative breast cancer using background parenchymal enhancement heterogeneity on dynamic contrast-enhanced MRI: A pilot radiomics study. PLOS ONE 10. https://doi.org/10.1371/journal.pone.0143308
32. Nie K, Shi L, Chen Q et al (2016) Rectal cancer: assessment of neoadjuvant chemoradiation outcome based on radiomics of multiparametric MRI. Clin Cancer Res 22:5256–5264
33. Aerts HJ, Velazquez ER, Leijenaar RT et al (2014) Decoding tumour phenotype by noninvasive imaging using a quantitative radiomics approach. Nat Commun 5:4006
34. Bayanati H, Thornhill RE, Souza CA et al (2014) Quantitative CT texture and shape analysis: Can it differentiate benign and malignant mediastinal lymph nodes in patients with primary lung cancer? Eur Radiol 25:480–487
35. Nie K, Chen JH, Yu HJ, Chu Y, Nalcioglu O, Su MY (2008) Quantitative analysis of lesion morphology and texture features for diagnostic prediction in breast MRI. Acad Radiol 15:1513–1525
36. Juntu J, Sijbers J, De Backer S, Rajan J, Van Dyck D (2010) Machine learning study of several classifiers trained with texture analysis features to differentiate benign from malignant soft-tissue tumors in T1-MRI images. J Magn Reson Imaging 31:680–689
37. Thornhill RE, Golfam M, Sheikh A et al (2014) Differentiation of lipoma from liposarcoma on MRI using texture and shape analysis. Acad Radiol 21:1185–1194
38. Fruehwald-Pallamar J, Hesselink JR, Mafee MF, Holzer-Fruehwald L, Czerny C, Mayerhoefer ME (2016) Texture-based analysis of 100 MR examinations of head and neck tumors - Is it possible to discriminate between benign and malignant masses in a multicenter trial? Rofo 188:195–202
39. Ding ZX, Lip G, Chong V (2011) Idiopathic orbital pseudotumour. Clin Radiol 66:886–892
40. Li Z, Mao Y, Li H, Yu G, Wan H, Li B (2015) Differentiating brain metastases from different pathological types of lung cancers using texture analysis of T1 postcontrast MR. Magne Reson Med 76: 1410–1419

41. Zhang B, Tian J, Dong D et al (2017) Radiomics features of multiparametric MRI as novel prognostic factors in advanced nasopharyngeal carcinoma. Clin Cancer Res 23:4259–4269
42. Ganeshan B, Abaleke S, Young RC, Chatwin CR, Miles KA (2010) Texture analysis of non-small cell lung cancer on unenhanced computed tomography: initial evidence for a relationship with tumour glucose metabolism and stage. Cancer Imaging 10:137–143
43. Ganeshan B, Miles KA, Young RC, Chatwin CR (2007) In search of biologic correlates for liver texture on portal-phase CT. Acad Radiol 14:1058–1068
44. Ganeshan B, Skogen K, Pressney I, Coutroubis D, Miles K (2012) Tumour heterogeneity in oesophageal cancer assessed by CT texture analysis: preliminary evidence of an association with tumour metabolism, stage, and survival. Clin Radiol 67:157–164
45. Ganeshan B, Panayiotou E, Burnand K, Dizdarevic S, Miles K (2012) Tumour heterogeneity in non-small cell lung carcinoma assessed by CT texture analysis: a potential marker of survival. Eur Radiol 22:796–802
46. Skogen K, Ganeshan B, Good C, Critchley G, Miles K (2013) Measurements of heterogeneity in gliomas on computed tomography relationship to tumour grade. J Neurooncol 111:213–219
47. Frighetto-Pereira L, Rangayyan RM, Metzner GA (2016) Shape, texture and statistical features for classification of benign and malignant vertebral compression fractures in magnetic resonance images. Computers in Biology & Medicine 73:147–156
48. Woods BJ, Clymer BD, Kurc T et al (2007) Malignant-lesion segmentation using 4D co-occurrence texture analysis applied to dynamic contrast-enhanced magnetic resonance breast image data. J Magn Reson Imaging 25:495–501
49. Sasaguri K, Takahashi N, Takeuchi M, Carter RE, Leibovich BC, Kawashima A (2016) Differentiation of benign from metastatic adrenal masses in patients with renal cell carcinoma on contrast-enhanced CT. AJR Am J Roentgenol 207:1031–1038
50. Fruehwald-Pallamar J, Czerny C, Holzer-Fruehwald L et al (2013) Texture-based and diffusion-weighted discrimination of parotid gland lesions on MR images at 3.0 Tesla. NMR Biomed 26: 1372–1379
51. Mueller-Using S, Feldt T, Sarfo FS, Eberhardt KA (2016) Factors associated with performing tuberculosis screening of HIV-positive patients in Ghana: LASSO-based predictor selection in a large public health data set. BMC Public Health 16:563
52. Gibbs P, Turnbull LW (2003) Textural analysis of contrast-enhanced MR images of the breast. Magn Reson Med 50:92–98
53. Xu R, Kido S, Suga K et al (2014) Texture analysis on (18)F-FDG PET/CT images to differentiate malignant and benign bone and soft-tissue lesions. Ann Nucl Med 28:926–935
54. Way TW, Hadjiiski LM, Sahiner B et al (2006) Computer-aided diagnosis of pulmonary nodules on CT scans: segmentation and classification using 3D active contours. Medical Physics 33:2323–2337
55. Sepahdari AR, Politi LS, Aakalu VK, Kim HJ, Razek AA (2014) Diffusion-weighted imaging of orbital masses: multi-institutional data support a 2-ADC threshold model to categorize lesions as benign, malignant, or indeterminate. AJNR Am J Neuroradiol 35: 170–175